Synthesis, Crystal Structure, Magnetic Susceptibility, and Mössbauer Spectroscopy of a Mixed-Valence Organic−Inorganic Hybrid Compound: $(H_3DETA)[Fe_3(C_2O_4)_2(HPO_4)_2(PO_4)]$ (DETA = Diethylenetriamine)

Yau-Chen Jiang,[†] Sue-Lein Wang,[†] and Kwang-Hwa Lii*[,‡,§]

Department of Chemistry, National Tsing Hua University, Hsinchu, Taiwan, Republic of China, Department of Chemistry, National Central University, Chungli, Taiwan, Republic of China, and Institute of Chemistry, Academia Sinica, Nankang, Taipei, Taiwan, Republic of China

Ninh Nguyen* and Annie Ducouret

Laboratoire CRISMAT, UMR CNRS 6508, ISMRA et Université de Caen, 14050 Caen Cedex, France

Received November 7, 2002. Revised Manuscript Received February 25, 2003

A mixed-valence organic−inorganic hybrid compound, $(H_3DETA)[Fe_3(C_2O_4)_2(HPO_4)_2(PO_4)]$ (DETA = diethylenetriamine), has been synthesized under hydrothermal conditions and characterized by single-crystal X-ray diffraction, magnetic susceptibility, ^{57}Fe powder absorption Mössbauer spectroscopy, and electric field gradient calculations. It crystallizes in the triclinic space group $P\bar{1}$ (No. 2) with $a = 9.6367(7)$ Å, $b = 10.1760(7)$ Å, $c = 12.6164(9)$ Å, $\alpha = 86.302(1)°$, $\beta = 68.880(1)°$, $\gamma = 61.800(1)°$, and $Z = 2$ with $R_1 = 0.0397$. The structure can be described as layers of trigonal bipyramidal $Fe^{II}O_5$, octahedral $Fe^{III}O_6$, tetrahedral PO_4 moieties, and monobidentate oxalate ligands, which are pillared through bisbidentate oxalate ligands to form a 3-D framework structure. The title compound is not only the first oxalatophosphate that contains two types of oxalate ligands but also the first example of mixed-valence transition metal oxalatophosphate.

Introduction

Recently, many researchers have studied the synthesis of hybrid frameworks by incorporating appropriate organic ligands into the structures of inorganic oxides.[1,2] As compared to the inorganic ligands such as phosphate and arsenate, the organic ligands have relatively larger sizes and more variety of means of connection. The organic components can dramatically influence the structures, thus providing a method for the design of new open-framework materials. One class of organic−inorganic hybrid compounds is based on 4,4′-bipyridine and phosphate in which the metal cations are coordinated by both types of ligands.[3−8] Another variant of metal phosphate is obtained by incorporating the oxalate unit into the structure. A large number of oxalatophosphates of V,[9−11] Mn,[12,13] Fe,[14−20] Al,[21,22] Ga,[23−25]

* Authors to whom correspondence should be addressed. E-mail: liikh@cc.ncu.edu.tw (K.-H.L.); ninh.nguyen@ismra.fr (N.N.)
[†] National Tsing Hua University.
[‡] National Central University.
[§] Academia Sinica.

(1) Hagrman, P. J.; Hagrman, D.; Zubieta, J. *Angew. Chem., Int. Ed.* **1999**, *38*, 2638 and references therein.
(2) Férey, G. *Chem. Mater.* **2001**, *13*, 3084 and references therein.
(3) Lii, K.-H.; Huang, Y.-F. *Inorg. Chem.* **1999**, *38*, 1348.
(4) Chen, C.-Y.; Lo, F.-R.; Kao, H.-M.; Lii, K.-H. *J. Chem. Soc., Chem. Commun.* **2000**, 1061.
(5) Shi, Z.; Feng, S.; Gao, S.; Zhang, L.; Yang, G.; Hua, J. *Angew. Chem. Int. Ed.* **2000**, *39*, 2325.
(6) Huang, C.-H.; Huang, L.-H.; Lii, K.-H. *Inorg. Chem.* **2001**, *40*, 2625.
(7) Jiang, Y.-C.; Lai, Y.-C.; Wang, S.-L.; Lii, K.-H. *Inorg. Chem.* **2001**, *40*, 5320.
(8) Huang, L.-H.; Kao, H.-M.; Lii, K.-H. *Inorg. Chem.* **2002**, *41*, 2936.
(9) Tsai, Y.-M.; Wang, S.-L.; Huang, C.-H.; Lii, K.-H. *Inorg. Chem.* **1999**, *38*, 4183.
(10) Do, J.; Bontchev, R. P.; Jacobson, A. J. *Inorg. Chem.* **2000**, *39*, 3230.
(11) Do, J.; Bontchev, R. P.; Jacobson, A. J. *Chem. Mater.* **2001**, *13*, 2601.
(12) Lethbridge, Z. A. D.; Hillier, A. D.; Cywinski, R.; Lightfoot, P. *J. Chem. Soc., Dalton Trans.* **2000**, 1595.
(13) Lethbridge, Z. A. D.; Tiwary, S. K.; Harrison, A.; Lightfoot, P. *J. Chem. Soc., Dalton Trans.* **2001**, 1904.
(14) Lin, H.-M.; Lii, K.-H.; Jiang, Y.-C.; Wang, S.-L. *Chem. Mater.* **1999**, *11*, 519.
(15) Lethbridge, Z. A. D.; Lightfoot, P. *J. Solid State Chem.* **1999**, *143*, 58.
(16) Choudhury, A.; Natarajan, S.; Rao, C. N. R. *J. Solid State Chem.* **1999**, *146*, 538.
(17) Choudhury, A.; Natarajan, S. *J. Mater. Chem.* **1999**, *9*, 3113.
(18) Choudhury, A.; Natarajan, S.; Rao, C. N. R. *Chem. Mater.* **1999**, *11*, 2316.
(19) Choudhury, A.; Natarajan, S.; Rao, C. N. R. *Chem. Eur. J.* **2000**, *6*, 1168.
(20) Chang, W.-J.; Lin, H.-M.; Lii, K.-H. *J. Solid State Chem.* **2001**, *157*, 233.
(21) Lightfoot, P.; Lethbridge, Z. A. D.; Morris, R. E.; Wragg, D. S. Wright, D. S.; Wright, P. A.; Kvick, Å Vaughan, G. B. M. *J. Solid State Chem.* **1999**, *143*, 74.
(22) Kedarnath, K.; Choudhury, A.; Natarajan, S. *J. Solid State Chem.* **2000**, *150*, 324.
(23) Chen, C.-Y.; Chu, P. P.; Lii, K.-H.*Chem. Commun.* **1999**, 1473.
(24) Lii, K.-H.; Chen, C.-Y. *Inorg. Chem.* **2000**, *39*, 3374.

10.1021/cm021701t CCC: $25.00
Published on Web 03/28/2003

In,[26] Sn,[27] and Zn[28] have been reported during the past few years. Most of these compounds consist of anionic 3-D frameworks templated with organic amines in protonated forms, while a few contain neutral frameworks without amine templates. In this class of organic−inorganic hybrid frameworks, there have been relatively more reports on transition metal compounds. The iron atoms in these compounds are either Fe^{III} or Fe^{II}. The vanadium and manganese atoms are in the oxidation state of +4 and +2, respectively. To our knowledge, mixed-valence transition metal oxalatophosphates have not been reported. Mixed-valence materials have been the subject of numerous studies because of their interesting magnetic and electric properties. This work describes the hydrothermal synthesis and structural characterization by single-crystal X-ray diffraction, magnetic susceptibility, and Mössbauer spectroscopy of the first example of mixed-valence transition metal oxalatophosphate, $(H_3DETA)[Fe_3(C_2O_4)_2(HPO_4)_2(PO_4)]$ (DETA = diethylenetriamine). In addition, the title compound consists of two types of oxalate ligands, which is a new structural feature in metal oxalatophosphate chemistry.

Experimental Section

Synthesis and Initial Characterization. The hydrothermal reactions were carried out in Teflon-lined stainless steel Parr acid digestion bombs. All chemicals were purchased from Aldrich Chemicals. A reaction of $FeCl_2 \cdot 4H_2O$ (0.298 g, 1.5 mmol), H_3PO_4 (85%, 1.326 g, 11.5 mmol), oxalic acid dihydrate (0.378 g, 3 mmol), diethylenetriamine (0.382 g, 3.7 mmol), and H_2O (12 mL) in a Teflon-lined acid digestion bomb at 165 °C for 3 days produced dark brown tablet crystals of $(H_3DETA)[Fe_3(C_2O_4)_2(HPO_4)_2(PO_4)]$, **1**. The initial and final pH values were 1.8 and 1.4, respectively. The product was filtered, washed with water, rinsed with ethanol, and dried in a desiccator at room temperature. The yield was 52% based on iron. Powder X-ray data were collected on a Shimadzu XRD-6000 automated powder diffractometer with Cu Kα radiation equipped with a scintillation detector. Data were collected in the range $5° \le 2\theta \le 50°$ using $\theta-2\theta$ mode in a flat-plate geometry. The powder pattern of the product is in good agreement with the calculated pattern based on the results from single-crystal X-ray diffraction (Figure 1). The program XPOW in the SHELXTL Version 5.1 software package was used for XRPD simulation.[29] Elemental analysis results are consistent with the stoichiometry of **1**. Anal. Found: C, 12.93; H, 2.71; N, 5.73%. Calcd: C, 13.04; H, 2.46; N, 5.70%. We also carried out retrosyntheses using $FeCl_2 \cdot 4H_2O$ and $FeCl_3 \cdot 4H_2O$ in a molar ratio of 1:2; the resulting products always contained a significant amount of the new compound $(H_3DETA)[Fe^{III}_4(OH)(C_2O_4)_{0.5}(HPO_4)_2(PO_4)_3]$ in addition to **1**.[30] It adopts a considerably different crystal structure.

Single-Crystal X-ray Diffraction. A suitable crystal of **1** with dimensions 0.15 × 0.10 × 0.06 mm was selected for indexing and intensity data collection on a Siemens SMART CCD diffractometer equipped with a normal focus, 3-kW sealed tube X-ray source. Intensity data were collected at room temperature in 1271 frames with ω scans (width 0.30° per frame). Empirical absorption corrections based on symmetry equivalents were applied.[31] The structure was solved by direct methods and difference Fourier syntheses. Bond-valence calculation results indicate that O(8) and O(12) are hydroxo oxygen atoms, Fe(1) and Fe(2) are trivalent, and Fe(3) is divalent.[32] The Fe−O bond lengths are similar to those in the mixed-valence iron phosphate $NH_4Fe_2(PO_4)_2$.[33] The H atoms in the hydroxo groups were located in difference Fourier maps. The H atoms, which are bonded to C atoms, were positioned geometrically and refined using a riding model with fixed isotropic thermal parameters. The H atoms bonded to N atoms were not located. The final cycles of least-squares refinement included atomic coordinates and anisotropic thermal parameters for all non-hydrogen atoms. The atomic coordinates and isotropic thermal parameters for all hydrogen atoms in the hydroxo groups were fixed. The final difference Fourier maps were flat ($\Delta\rho_{max,min} = 0.84, -0.46$ e/Å^3). All calculations were performed using the SHELXTL Version 5.1 software package.[29]

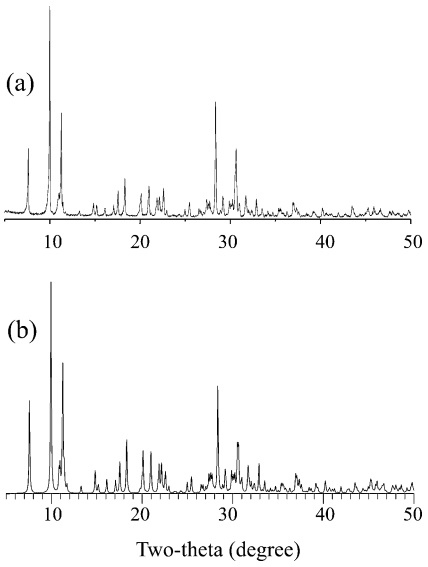

Figure 1. (a) X-ray powder pattern of **1**. (b) Simulated powder pattern from the atomic coordinates derived from single-crystal X-ray diffraction.

Magnetic Susceptibility and Mössbauer Measurements. Magnetic susceptibilities were measured using a dc SQUID system with a magnetic field of 0.3 T. The ^{57}Fe powder absorption Mössbauer spectra were recorded at 4.5 K, 80 K, and room temperature with a $^{57}Co/Rh$ source and a conventional constant acceleration Mössbauer spectrometer. The spectra were least-squares fitted using the computer program MOSFIT.[34] The isomer shift values are relative to iron metal at 293 K.

Results and Discussion

Description of the Structure. The crystal data and structure refinement parameters are given in Table 1 and selected bond distances in Table 2. Figure 2 shows the local coordination of the framework atoms and the organic template molecule. Both Fe(1) and Fe(2) are trivalent and are in six-coordination with a distorted

(25) Hung, L.-C.; Kao, H.-M.; Lii, K.-H. *Chem. Mater.* **2000**, *12*, 2411.
(26) Huang, Y.-F.; Lii, K.-H. *J. Chem. Soc., Dalton Trans.* **1998**, 4085.
(27) Natarajan, S. *J. Solid State Chem.* **1998**, *139*, 200.
(28) Neeraj, S.; Natarajan, S.; Rao, C. N. R. *J. Chem. Soc., Dalton Trans.* **2001**, 289.
(29) Sheldrick, G. M. *SHELXTL Programs*, version 5.1; Bruker AXS GmbH: Karlsruhe, Germany, 1998.
(30) Crystal data for $(H_3DETA)[Fe^{III}_4(OH)(C_2O_4)_{0.5}(HPO_4)_2(PO_4)_3]$: orthorhombic, *Pbcn*, $a = 22.810(1)$ Å, $b = 8.1299(3)$ Å, $c = 23.059(1)$ Å. A single-phase product of this Fe^{III} oxalatophosphate was synthesized by using $FeCl_3 \cdot 6H_2O$ as a starting material. Its 3-D framework structure consists of infinite chains of edge- and corner-sharing FeO_6 octahedra linked by FeO_5 trigonal bipyramids and phosphate tetrahedra to generate channels along the *b*- and *c*-axis. The oxalate unit shows a bisbidentate coordination to iron atoms.
(31) Sheldrick, G. M. *SADABS*; Siemens Analytical X-ray Instrument Division: Madison, WI, 1995.
(32) Brown, I. D.; Altermatt, D. *Acta Crystallogr.* **1985**, *B41*, 244.
(33) Boudin, S.; Lii, K.-H. *Inorg. Chem.* **1998**, *37*, 799.
(34) Teillet, J.; Varret, F. *MOSFIT Program*; Université du Maine: France, unpublished.

Table 1. Crystallographic Data for $(H_3DETA)[Fe_3(C_2O_4)_2(HPO_4)_2(PO_4)]$

chemical formula	$C_8H_{18}N_3O_{20}P_3Fe_3$
crystal system	triclinic
space group	$P\bar{1}$ (No. 2)
a, Å	9.6367(7)
b, Å	10.1760(7)
c, Å	12.6164(9)
α, deg	86.302(1)
β, deg	68.880(1)
γ, deg	61.800(1)
V, Å^3	1008.66
Z	2
fw	736.72
T, K	296
λ(Mo Kα), Å	0.71073
ρ_{calc}, g·cm^{-3}	2.426
μ(Mo Kα), cm^{-1}	24.8
$2\theta_{max}$	56.6
unique data ($I > 2\sigma(I)$)	4053
no. of variables	335
R1[a]	0.0397
wR2[b]	0.0977
$(\Delta\rho)_{max,min}$	0.84, −0.46

[a] $R1 = \Sigma||F_o| - |F_c||/\Sigma|F_o|$. [b] $wR2 = \Sigma\{[w(F_o^2 - F_c^2)^2]/\Sigma[w(F_o^2)^2]\}^{1/2}$, $w = 1/[\sigma^2(F_o^2) + (aP)^2 + bP]$, $P = [Max(F_o,0) + 2(F_c)^2]/3$, where $a = 0.0395$ and $b = 3.09$.

Table 2. Bond Lengths (Å) and Bond Valence Sums (Σs) for $(H_3DETA)[Fe_3(C_2O_4)_2(HPO_4)_2(PO_4)]$[a]

Fe(1)−O(2)	1.928(2)	Fe(1)−O(5)	1.955(2)
Fe(1)−O(6)	1.982(2)	Fe(1)−O(11)	1.994(2)
Fe(1)−O(13)	2.086(3)	Fe(1)−O(15)	2.072(3)
Σs(Fe(1)−O) = 3.14			
Fe(2)−O(1)	1.955(2)	Fe(2)−O(7)	2.068(2)
Fe(2)−O(9)	1.940(2)	Fe(2)−O(10)	1.961(2)
Fe(2)−O(17)	2.070(3)	Fe(2)−O(19)	2.046(3)
Σs(Fe(2)−O) = 3.11			
Fe(3)−O(3)	2.025(3)	Fe(3)−O(4)	2.020(3)
Fe(3)−O(7)	2.100(2)	Fe(3)−O(14)	2.098(3)
Fe(3)−O(16)	2.197(3)		
Σs(Fe(3)−O) = 1.95			
P(1)−O(1)	1.536(2)	P(1)−O(2)	1.548(2)
P(1)−O(3)	1.522(3)	P(1)−O(4)	1.534(3)
Σs(P(1)−O) = 4.98			
P(2)−O(5)	1.508(2)	P(2)−O(6)	1.518(3)
P(2)−O(7)	1.540(3)	P(2)−O(8)	1.571(3)
Σs(P(2)−O) = 5.01			
P(3)−O(9)	1.510(3)	P(3)−O(10)	1.528(2)
P(3)−O(11)	1.526(2)	P(3)−O(12)	1.577(3)
Σs(P(3)−O) = 5.00			
C(1)−O(13)	1.250(4)	C(1)−O(14)	1.250(4)
C(2)−O(15)	1.258(4)	C(2)−O(16)	1.238(4)
C(3)−O(17)	1.264(4)	C(3)−O(18)	1.230(4)
C(4)−O(19)	1.266(4)	C(4)−O(20)	1.232(5)
C(5)−C(6)	1.523(6)	C(5)−N(1)	1.489(5)
C(6)−N(2)	1.505(5)	C(7)−C(8)	1.517(6)
C(7)−N(2)	1.489(5)	C(8)−N(3)	1.484(6)

[a] The C−H bond lengths are given in the Supporting Information.

octahedral geometry, but they do not display the same coordination environment. Fe(1) is coordinated by one bisbidentate oxalate chelate, one PO_4, and three HPO_4 ligands, while Fe(2) by one monobidentate oxalate chelate, one PO_4, and three HPO_4 ligands. Fe(3) is divalent and is in five-coordination with a strongly distorted trigonal bipyramid geometry. $Fe(2)O_6$, $Fe(3)O_5$, and $HP(2)O_4$ polyhedra share a common corner, O(7). The title compound should be a member of the class I system in the Robin-Day scheme because the trivalent and divalent iron atoms are in very different coordination environments. There are two distinct oxalate ligands in the structure: $C(1)C(2)O_4$ is a bisbidentate chelate which bridges $Fe(1)^{III}$ and $Fe(3)^{II}$, whereas $C(3)C(4)O_4$ is a monobidentate chelate to $Fe(2)^{III}$ as a terminal ligand. The Fe−O bonds between Fe(3) and the oxalate are the longest because the radius of Fe^{II} is larger than that of Fe^{III}, although the cation radius increases with increasing coordination number. The Fe−O bonds between Fe(2) and the monobidentate oxalate are the shortest. The increase of the following bite angles of oxalate ligands is due to the increase in repulsion between two oxygen anions with decreasing Fe−O bond lengths: O−Fe(3)−O, 77.5(1)°; O−Fe(1)−O, 78.6(1)°; O−Fe(2)−O, 79.0(1)°.

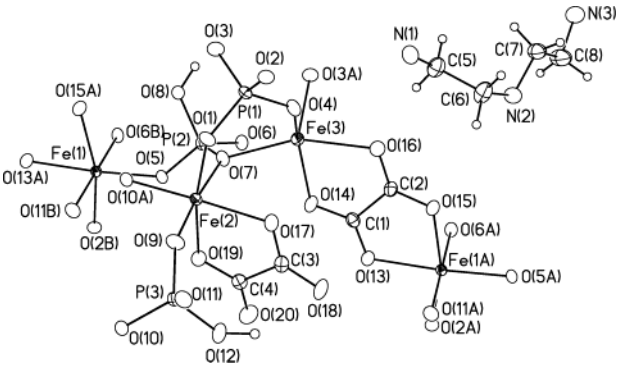

Figure 2. A fragment of the structure of **1** showing the organic template molecule and the connectivity among the structural building units. Thermal ellipsoids are given at 50% probability. Small open circles are H atoms. The H atoms bonded to N atoms are not shown.

There are three distinct phosphate tetrahedra. $P(1)O_4$ is connected to four Fe−O polyhedra at four vertexes. $HP(2)O_4$ and $HP(3)O_4$ are linked through three oxygens to four and three adjacent Fe atoms, respectively, with the fourth coordination site in either case corresponding to a terminal P−OH group. One of the three oxygen atoms in $HP(2)O_4$, O(7), connects two iron atoms. The P−OH groups are involved in hydrogen bonding as indicated from the short H···O and O···O distances (H(8O)···O(4), 1.75 Å; O(8)···O(4), 2.63 Å; H(12O)···O(18), 1.68 Å; O(12)···O(18), 2.62 Å).

Compound **1** is constructed from $Fe^{II}O_5$, $Fe^{III}O_6$, and phosphate polyhedra and oxalate units. These iron polyhedra and phosphate tetrahedral are linked to each other via corner sharing to form iron phosphate layers in the *ac* plane (Figure 3). The oxalate units $C(1)C(2)O_4$ show bisbidentate coordination to Fe(1) and Fe(3), acting as pillars between adjacent layers to produce the extended three-dimensional network (Figure 4). The other oxalate unit $C(3)C(4)O_4$ shows a monobidentate coordination to Fe(2) as a terminal ligand and protrudes into the interlayer space. There is hydrogen bonding between $C(3)C(4)O_4$ and $HP(3)O_4$ units in adjacent layers. Eight-ring channels formed by the edges of four FeO_6 octahedra and four phosphate tetrahedra are found in the *b* direction which contain triprotonated diethylenetriamine, located between adjacent layers. The cations are hydrogen-bonded to the framework via N−H···O bonds as inferred from several N···O distances shorter than 2.9 Å.

Three different types of oxalate coordination are observed in the structures of metal oxalatophosphates reported, namely, bisbidentate, monobidentate, and bismono- and bisbidentate, as indicated by Lightfoot and co-workers.[21] The bisbidentate coordination is very

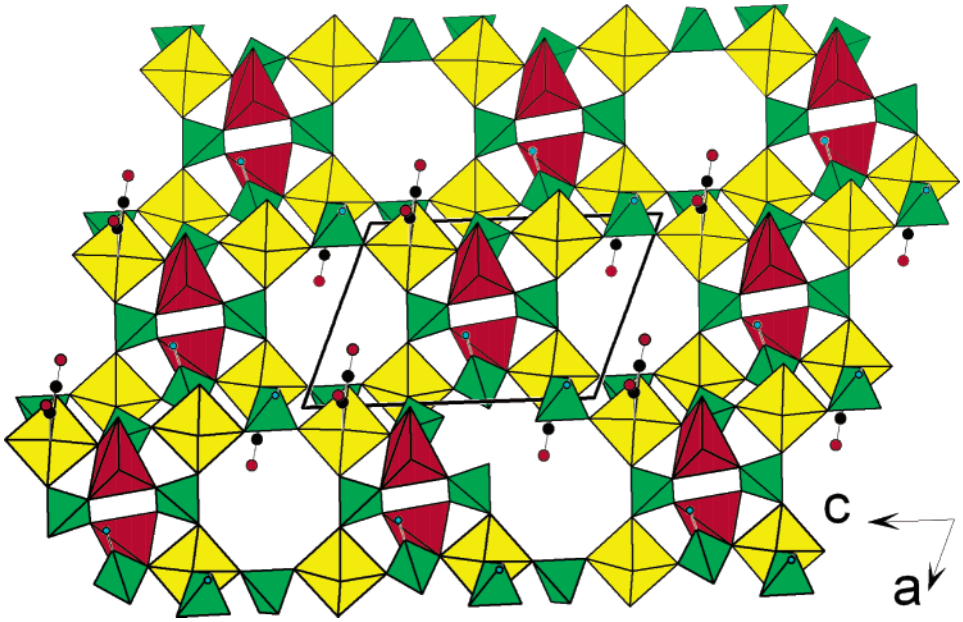

Figure 3. Section of a sheet of the structure of **1** viewed along [010]. FeO_6 octahedra, FeO_5 trigonal bipyramids, and phosphate tetrahedra are shown in yellow, red, and green, respectively. Black circles, C atoms; red circles, O atoms; small blue circles, H atoms.

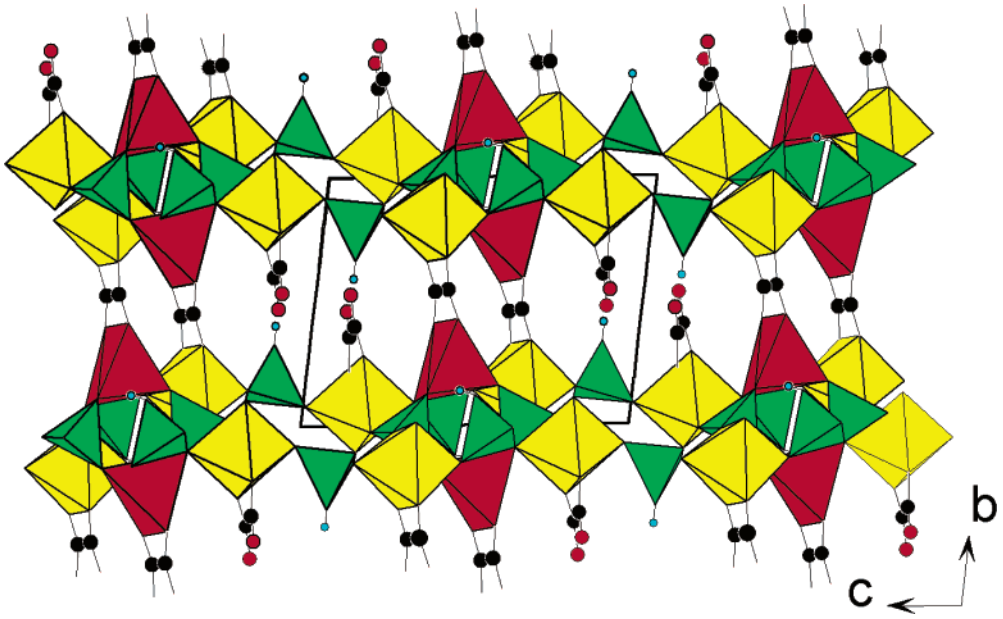

Figure 4. A polyhedral view of the structure of **1** along the [100] direction.

common and is seen in 90% of the structures. Many of these compounds can be described as metal phosphate layers pillared by oxalate anions. The monobidentate coordination is less common and is seen in the one-dimensional $[NH_3CH_2CH_2NH_3]_{2.5}[Al_4H(C_2O_4)_4(H_2PO_4)_2(HPO_4)_4]$ and $[C_4H_{12}N_2][VO(C_2O_4)(HPO_4)]$ where the oxalate anion caps the metal atoms and allows hydrogen bonding between the chains. Bismono- and bisbidentate coordination by the same oxalate anion is observed in $[Fe_2(C_2O_4)_{0.5}(PO_4)(H_2O)]$. The title compound consists of two types of oxalate groups which act as bisbidentate and monobidentate ligands to iron atoms. It presents a new structural feature in metal oxalatophosphate chemistry.

Magnetic Susceptibility. The temperature dependence of $\chi_M T$ and $1/\chi_M$ curves, where χ_M is the molar magnetic susceptibility, are shown in Figure 5. The

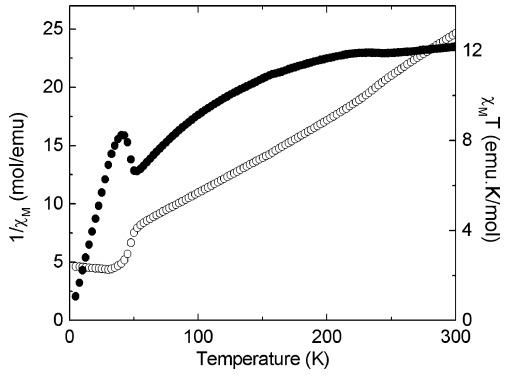

Figure 5. dc magnetic susceptibility $1/\chi_M$ (open circles) and $\chi_M T$ (solid circles) versus temperature registered under 0.3 T.

effective magnetic moment at 300 K is $2.83(\chi_M T)^{1/2} = 9.86\ \mu_B$ as compared with the spin-only value of

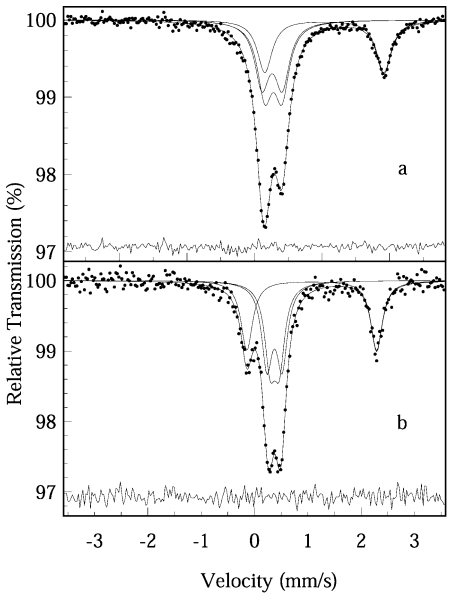

Figure 6. ^{57}Fe powder Mössbauer spectra recorded at (a) 293 K and (b) 80 K.

Table 3. Fitted Hyperfine Mössbauer Parameters for $(H_3DETA)[Fe_3(C_2O_4)_2(HPO_4)_2(PO_4)]$ at 293 and 80 K

T (K)	site	IS ± 0.01 (mm·s^{-1})	Γ ± 0.01[a] (mm·s^{-1})	|QS| ± 0.01 (mm·s^{-1})	% ± 3	iron charge
293	A	0.39	0.13	0.25	38	+3
	A′	0.37	0.13	0.30	33	+3
	B	1.15	0.13	1.76	29	+2
80	A	0.49	0.12	0.17	32	+3
	A′	0.49	0.12	0.28	35	+3
	B	1.19	0.13	2.43	33	+2

[a] Γ is the half-width at half-maximum of the observed resonance line.

$(5 \times 7 \times 2 + 4 \times 6)^{1/2} = 9.70\ \mu_B$, which is in good agreement with the presence of one Fe^{2+} and two Fe^{3+} ions considering that the magnetic moments of Fe^{2+} complexes at room temperature are generally in the range from 5.1 to 5.5 μ_B Upon cooling, the antiferromagnetic ordering appears at about 45 K as evidenced by the $1/\chi_M$ vs T curve, $\theta_p \approx -40$ K. The magnetic interaction could be due to the superexchange coupling between $Fe(2)^{III}$ and $Fe(3)^{II}$ via O(7) and between $Fe(1)^{III}$ and $Fe(3)^{II}$ via the bisbidentate oxalate ligand. The interaction between $Fe(1)^{III}$ and $Fe(2)^{III}$ is less probable because the two iron atoms are separated by a phosphate group.

Mössbauer Spectroscopy and EFG Calculations. The room-temperature Mössbauer powder spectrum (Figure 6a) of the sample indicates the presence of pure electric quadrupole interactions and the spectrum was fitted by means of classical symmetric Lorentzian doublets. The fit was obtained from a decomposition of the spectrum into three main quadrupole sites noted as A, A′, and B in Table 3. The isomer shift (IS) values for A and A′ sites are 0.39 and 0.37 mm·s^{-1}, respectively, which are typical of trivalent iron. The value for the B site is 1.15 mm·s^{-1}, indicating a divalent iron. Furthermore, the observed relative intensities lead to a ratio of $Fe^{3+}(A + A')/ Fe^{2+}(B) \approx 70/30$, in agreement with the existence of the $Fe(1)^{3+}$, $Fe(2)^{3+}$, and $Fe(3)^{2+}$ crystallographic sites in equal proportion. The fit also leads to absolute values of quadrupole splitting |S| of 0.25 and 0.30 mm·s^{-1} for A and A′ components, respectively. However, these results do not allow us to differentiate between Fe(1) and Fe(2), for which the coordination environments are different. Electric field gradient (EFG) calculation could be useful because it takes account of the role played by the various anisotropic environments of $Fe(1)^{3+}$ and $Fe(2)^{3+}$ ions upon their Mössbauer hyperfine parameters and then determines the theoretical algebraic lattice quadrupole splittings $(QS)_{lat}$ and the asymmetry parameters η of these sites.

Table 4. EFG Lattice Calculation Results at 293 K for Fe^{3+} Ions

site	QS_{lat} ± 0.01 (mm·s^{-1})	η ± 0.02	Z orientation[a]		
$Fe(1)^{3+}$	±0.73[b]	0.99	−0.1947[b]	0.9591[b]	−0.2055[b]
$Fe(2)^{3+}$	0.62	0.63	0.8482	−0.1748	0.4950

[a] Cosines of the principal Z direction of the EFG gradient. Results are given in the International Orthonormal Reference frame ($\mathbf{e}_1$, $\mathbf{e}_2$, $\mathbf{e}_3$) related to the crystallographic frame (**a**,**b**,**c**) by $\mathbf{e}_1$ // **a**, $\mathbf{e}_2$ in the (**a**,**b**) plane, and $\mathbf{e}_3 \perp (\mathbf{e}_1,\mathbf{e}_2)$. [b] Because η is very close to 1, $V_{ZZ} \approx -V_{YY}$, it is difficult to be precise with the sign for QS_{lat}. The given Z orientation in this table corresponds to the positive sign.

We have performed room-temperature EFG calculations at the iron sites, limited to the point charge contributions of all the ions in the whole crystal[35] with the $P\bar{1}$ space group to respect the neutral state of the molecule. For the Fe^{3+} sites, the $3d^5$ electronic valence shells are nearly symmetric; thus, the whole $[\mathbf{V}_{ij}] = [\mathbf{V}_{ij}]_{lat} + [\mathbf{V}_{ij}]_{val}$ EFG tensors are well approximated by the $[\mathbf{V}_{ij}]_{lat}$ contributions alone.

Using the room-temperature cell parameters and atomic positions, we have calculated the components of the $[\mathbf{V}_{ij}]_{lat}$ tensors in the international orthonormal reference frame (IOR) ($\mathbf{e}_1$ // **a**, $\mathbf{e}_2$ in the (**a**,**b**) plane, $\mathbf{e}_3 \perp (\mathbf{e}_1,\mathbf{e}_2)$). After diagonalization of these tensors, we obtained their respective eigenvalues V_{XX}^{lat}, V_{YY}^{lat}, V_{ZZ}^{lat} (with $|V_{XX}^{lat}| < |V_{YY}^{lat}| < |V_{ZZ}^{lat}|$) and the directions X, Y, Z of their principal axes in the IOR frame.

The asymmetry parameters η_1, η_2 ($0 \le \eta = (V_{XX} - V_{YY})/V_{ZZ} \le 1$) and the orientation of the EFG tensor principal axes can then be deduced for both $Fe(1)^{3+}$ and $Fe(2)^{3+}$. The quadrupole splitting of the paramagnetic room-temperature Mössbauer doublets can be determined for the two Fe^{3+} sites using $QS \approx QS_{lat} = (1 - \gamma_\infty)\ (eQ/2)V_{ZZ}^{lat}\ (1 + \eta^2/3)^{1/2}$, where $(1 - \gamma_\infty) \approx 10.14$ is the Sternheimer antishielding factor[36] and $Q \approx 0.2$ barn[37,38] is the nuclear quadrupole moment of ^{57}Fe in the excited $I = {}^3/_2$ state.

The EFG calculation results for $Fe(1)^{3+}$ and $Fe(2)^{3+}$ sites are given in Table 4. The calculated |QS| values are higher than the experimental ones. This is not surprising owing to the approximation of a point charge model which does not account for the effects of multipolar terms on the iron nuclei in the development of an electric field gradient. These terms might not be negligible in a covalent compound. However, the difference between the two calculated values of |QS| is similar to

(35) Calage, Y.; Teillet, J.; Varret, F. *"EFGDIR" program for lattice EFG tensors*; Université du Maine: France, 1982.
(36) Ingalls, R. *Phys. Rev.* **1962**, *128*, 1155.
(37) Sternheimer, R. M. *Phys. Rev.* **1953**, *92*, 1460.
(38) Gütlich, P.; Link, R.; Trautwein, A. *Inorganic Chemistry Concepts, Vol. 3, Mössbauer Spectroscopy and Transition Metal Chemistry*; Spinger Verlag: Berlin, 1978.

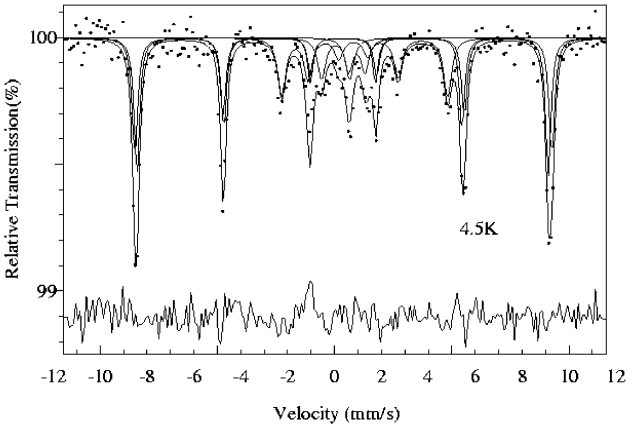

Figure 7. ^{57}Fe powder Mössbauer spectrum recorded at 4.5 K.

Table 5. Fitted Hyperfine Mössbauer Parameters for $(H_3DETA)[Fe_3(C_2O_4)_2(HPO_4)_2(PO_4)]$ at 4.5 K

site	IS ± 0.01 (mm·s^{-1})	2ϵ ± 0.01[a] (mm·s^{-1})	H_f ± 0.1 (T)	% ± 4	iron charge
A	0.49	−0.02	55.2	31	+3
A′	0.46	−0.01	54.5	33	+3
B	1.15	0.88	21.5	23	+2
	0.16	1.20[b]		7	+3
	1.06	0.70[b]		6	+2

[a] 2ϵ is quadrupole shift. [b] Quadrupole splitting values (QS) of paramagnetic components.

the experimental one ($|QS_1| - |QS_2| = 0.11$ and $|QS_{A'}| - |QS_A| = 0.05$ mm·s^{-1}). This allows us to attribute the Mössbauer A site to Fe(2) and the A′ site to Fe(1). Note that the $\eta(1)$ value is also greater than $\eta(2)$ ($\eta_1 = 0.99$, $\eta_2 = 0.63$), indicating a more distorted environment for Fe(1). This is consistent with the first-order octahedral distortions of these sites, which can be estimated by using the equation $\Delta = (1/6)\Sigma[(R_i - R_{av})/R_{av}]^2$, where R_i are the individual Fe−O bond lengths and R_{av} is the average bond length[39] ($10^4 \times \Delta = 8.4$ and 7.6 for Fe(1)O_6 and Fe(2)O_6, respectively).

The paramagnetic Mössbauer spectrum performed at 80 K (Figure 6b) shows that the QS value of Fe^{2+} site is very different from the room-temperature one (Table 3), in agreement with the usually observed large thermal variation of the $[\mathbf{V}_{ij}]_{val}$ tensor due to thermal population of the $3d^6$ electronic levels. With regard to the A and A′ sites, the variations of QS between 293 and 80 K are small (Table 3) because only the lattice term, whose thermal variation is small, contributes to the QS values.

The 4.5 K Mössbauer spectrum (Figure 7) is magnetic, in agreement with the magnetic susceptibility results. It can be fitted with three main magnetic components whose IS and hyperfine field (H_f) values confirm the presence of two Fe^{3+} (IS = 0.49 and 0.46 mm·s^{-1}, H_f = 55.2 and 54.5 T) and one Fe^{2+} (IS = 1.15 mm·s^{-1}, H_f = 21.5 T) (Table 5). These sites correspond respectively to A, A′, and B sites observed in the paramagnetic domain. Note that there are two small paramagnetic contributions of Fe^{3+} (IS = 0.16 mm·s^{-1}) and Fe^{2+} (IS = 1.06 mm·s^{-1}) with relative intensities of about 6%. They could be attributed to the existence of some superparamagnetic iron clusters in the magnetic phase.

In summary, we have reported the hydrothermal synthesis and structural characterization of a new iron phosphatooxalate. Its 3-D framework structure consists of two types of oxalate groups which act as bisbidentate and monobidentate ligands to iron atoms. The former connects Fe^{III} and Fe^{II} and the latter coordinates to Fe^{III} as a terminal ligand. We have also performed magnetic susceptibility and Mössbauer spectroscopy measurements and EFG calculations to confirm the valence and stoichiometry of the iron atoms as indicated from crystal structure analysis. The title compound is not only the first oxalatophosphate that contains two types of oxalate ligands but also the first example of mixed-valence transition metal oxalatophosphates.

We aim to combine the flexibility of metal organic coordination systems with the tetrahedral phosphate anions to produce new open framework structures. The isolation of the 3-D covalent framework material (H_3-DETA)$[Fe_3(C_2O_4)_2(HPO_4)_2(PO_4)]$ illustrates once again that oxalate and phosphate anions can be employed as structural building units in the synthesis of organic−inorganic hybrid compounds. Furthermore, the coordination preferences of the metal centers also contribute to the ultimate framework geometry, as evidenced by the octahedral geometry at the Fe^{III} site and trigonal bipyramidal geometry at the Fe^{II} site. It is evident that other factors such as the identity of countercations contribute to the design of solid-state architectures. It is also interesting to explore mixed metal materials where the two metals have different coordination preferences and order on different crystallographic sites. Further work on these themes is in progress.

Acknowledgment. The authors (Y.-C.J., S.-L.W., and K.-H.L.) thank the National Science Council of Taiwan for support and Dr. A. Maignan from Laboratoire CRISMAT for magnetic susceptibility measurements.

Supporting Information Available: Tables of crystal data, atomic coordinates, bond distances, bond angles, and anisotropic thermal parameters (PDF). One crystallographic information file (CIF). This material is available free of charge via the Internet at http://pubs.acs.org.

CM021701T

(39) Shannon, R. D. *Acta Crystallogr.* **1976**, *A32*, 751.